European Conference on Computational Fluid Dynamics
ECCOMAS CFD 2006
P. Wesseling, E. Oñate and J. Périaux (Eds)

ERROR ESTIMATION AND ADJOINT-BASED ADAPTATION IN AERODYNAMICS

Ralf Hartmann*

* German Aerospace Center (DLR)
Institute of Aerodynamics and Flow Technology (AS)
Lilienthalplatz 7, 38108 Braunschweig
e-mail: Ralf.Hartmann@dlr.de
web page: http://www.dlr.de/as

Key words: Error estimation, Adjoint-based refinement, Discontinuous Galerkin discretization, Compressible flows, Aerodynamics

Abstract. *In this article we give an overview of recent developments in error estimation and in residual-based and goal-oriented (adjoint-based) adaptation for Discontinuous Galerkin discretizations of sub- and supersonic viscous compressible flows. We also give an outlook on the planned continuation of this research in the EU project ADIGMA.*

1 INTRODUCTION

In aerodynamical computations like compressible flows around airfoils, much emphasis is placed on the accurate approximation of specific target quantities $J(\cdot)$, in particular, the aerodynamical force coefficients like the pressure induced as well as the viscous stress induced drag, lift and moment coefficients, respectively. While local mesh refinement is required for obtaining reasonably accurate results in applications, the goal of the adaptive refinement is either to compute these coefficients as accurate as possible within given computing resources or to compute these coefficients up to a given tolerance with the minimum computing resources required. In both cases a goal-oriented refinement is needed, i.e. an adaptive refinement strategy specifically targeted to the efficient computation of the quantities of interest. Furthermore, in the latter case, an estimate is required of how accurate the force coefficients are approximated, i.e. an *a posteriori* error estimate is required of the error of the numerical solution measured in terms of the quantity of interest.

This error can be represented by the element and face residuals of the primal (flow) solution multiplied by the solution of a dual (adjoint) problem with data coupling to the specific target quantity. By approximating the solution to the dual problem numerically, the resulting approximate error representation gives an estimate of the true error. Furthermore, the approximate error representation can be decomposed as a sum over all elements of *adjoint-based* (also called *dual-weighted residual*) indicators which can

be used for goal-oriented (adjoint-based) refinement specifically tailored to the efficient computation of the quantities of interest.

The approach of *a posteriori* error estimation and adaptivity in finite element methods has been developed in [1] and applied to various kinds of problems, see the survey article [2]. In [4], this approach has been developed for the discontinuous Galerkin discretization of scalar hyperbolic problems. Then, in the series of publications, [5, 7, 8], it has been extended to the two–dimensional compressible Euler equations, where a variety of problems have been considered, including the Ringleb flow problem, supersonic flow past a wedge, inviscid flows through a nozzle, and inviscid sub-, trans- and supersonic flows around different airfoil geometries; finally, in [9] and [10], this approach has been extended to the two–dimensional compressible Navier-Stokes equations and applied to subsonic viscous compressible flows around simple airfoil geometries. [6] gives the extension of this approach to viscous compressible flows including shocks, like supersonic flows, for example.

In this publication we give an overview of recent developments in the *a posteriori* error estimation as well as residual-based and goal-oriented (adjoint-based) adaptation for Discontinuous Galerkin discretizations of sub- and supersonic compressible flows. First we present an overview of the general theoretical framework of duality-based (adjoint-based) *a posteriori* error estimation in Section 2. Then, we introduce the Discontinuous Galerkin (DG) discretization of the compressible Euler equations in Section 3 and the Interior Penalty DG discretization of the compressible Navier-Stokes equations in Section 4 and give the corresponding residual-based and adjoint-based refinement indicators used for adaptive mesh refinement. Then, in Section 5 we present some numerical examples highlighting the quality of the *a posteriori* error estimation and the advantage of using adjoint-based mesh refinement over residual-based mesh refinement. In the concluding Section 6 we give an outlook on the further development of these algorithms for the use in aerodynamical applications as planned in the EU project ADIGMA.

2 A POSTERIORI ERROR ESTIMATION

In this section we give an overview of the general theoretical framework of duality-based (adjoint-based) *a posteriori* error estimation developed by C. Johnson and R. Rannacher and their collaborators, [1, 2, 3] and the references cited therein.

Let $\mathbf{V}$ be a Hilbert space. Further, we write $\mathcal{N}(\cdot,\cdot)$ to denote a semi-linear form (nonlinear in its first argument, but linear in its second), with derivative $\mathcal{N}'_{\mathbf{u}}(\cdot;\cdot,\cdot)$. We suppose that $\mathbf{u}$ is the unique solution to the variational problem: find $\mathbf{u}$ in $\mathbf{V}$ such that

$$\mathcal{N}(\mathbf{u},\mathbf{v}) = 0 \quad \forall \mathbf{v} \in \mathbf{V}. \tag{1}$$

In order to construct a Galerkin approximation to this problem, we consider a sequence of finite–dimensional spaces $\{\mathbf{V}_h\}$, parameterized by the positive discretization parameter h; for the sake of simplicity we suppose that $\mathbf{V}_h \subset \mathbf{V}$ for each h. For the purposes of this paper, $\mathbf{V}_h$ can be thought of as finite element spaces consisting of piecewise polynomial

functions on a partition, of granularity h, of the computational domain. The Galerkin approximation $\mathbf{u}_h$ of $\mathbf{u}$ is then sought in $\mathbf{V}_h$ as the solution of the finite–dimensional problem

$$\mathcal{N}(\mathbf{u}_h, \mathbf{v}_h) = 0 \quad \forall \mathbf{v}_h \in \mathbf{V}_h. \tag{2}$$

For simplicity of presentation, we assume that $\mathbf{V}_h$ is a suitably chosen finite element space to ensure the existence of a unique solution $\mathbf{u}_h$ to (2). Furthermore, we assume that the discretization (2) is consistent, i.e. the exact solution $\mathbf{u}$ of (1) satisfies the discrete problem, i.e.

$$\mathcal{N}(\mathbf{u}, \mathbf{v}_h) = 0 \quad \forall \mathbf{v}_h \in \mathbf{V}_h. \tag{3}$$

Combining (2) and (3) we obtain the so-called Galerkin orthogonality of the discretization:

$$\mathcal{N}(\mathbf{u}, \mathbf{v}_h) - \mathcal{N}(\mathbf{u}_h, \mathbf{v}_h) = 0 \quad \forall \mathbf{v}_h \in \mathbf{V}_h, \tag{4}$$

which will be a key ingredient in the following *a posteriori* error analysis.

Assuming that the functional of interest $J(\cdot)$ is differentiable with derivative $J'[\mathbf{w}](\cdot)$ at some $\mathbf{w}$ in $\mathbf{V}$, we write $\bar{J}(\mathbf{u}, \mathbf{u}_h; \cdot)$ to denote the mean value linearization of $J(\cdot)$ defined by

$$\bar{J}(\mathbf{u}, \mathbf{u}_h; \mathbf{u} - \mathbf{u}_h) = J(\mathbf{u}) - J(\mathbf{u}_h) = \int_0^1 J'[\theta\mathbf{u} + (1-\theta)\mathbf{u}_h](\mathbf{u} - \mathbf{u}_h)\,\mathrm{d}\theta, \tag{5}$$

Analogously, we write $\mathcal{M}(\mathbf{u}, \mathbf{u}_h; \cdot, \cdot)$ to denote the mean–value linearization of $\mathcal{N}(\cdot, \cdot)$ given by

$$\begin{aligned} \mathcal{M}(\mathbf{u}, \mathbf{u}_h; \mathbf{u} - \mathbf{u}_h, \mathbf{v}) &= \mathcal{N}(\mathbf{u}, \mathbf{v}) - \mathcal{N}(\mathbf{u}_h, \mathbf{v}) \\ &= \int_0^1 \mathcal{N}'_{\mathbf{u}}[\theta\mathbf{u} + (1-\theta)\mathbf{u}_h](\mathbf{u} - \mathbf{u}_h, \mathbf{v})\,\mathrm{d}\theta \end{aligned} \tag{6}$$

for all $\mathbf{v}$ in $\mathbf{V}$. We now introduce the following *dual problem* (or adjoint problem): find $\mathbf{z} \in \mathbf{V}$ such that

$$\mathcal{M}(\mathbf{u}, \mathbf{u}_h; \mathbf{w}, \mathbf{z}) = \bar{J}(\mathbf{u}, \mathbf{u}_h; \mathbf{w}) \quad \forall \mathbf{w} \in \mathbf{V}. \tag{7}$$

For the proceeding error analysis, we assume that the dual problem (7) is well–posed. Under this assumption, employing the Galerkin orthogonality property (4) we deduce the following error representation formula:

$$\begin{aligned} J(\mathbf{u}) - J(\mathbf{u}_h) &= \bar{J}(\mathbf{u}, \mathbf{u}_h; \mathbf{u} - \mathbf{u}_h) \\ &= \mathcal{M}(\mathbf{u}, \mathbf{u}_h; \mathbf{u} - \mathbf{u}_h, \mathbf{z}) \\ &= \mathcal{M}(\mathbf{u}, \mathbf{u}_h; \mathbf{u} - \mathbf{u}_h, \mathbf{z} - \mathbf{z}_h) \\ &= -\mathcal{N}(\mathbf{u}_h, \mathbf{z} - \mathbf{z}_h) \end{aligned} \tag{8}$$

for all $\mathbf{z}_h$ in the finite element space $\mathbf{V}_h$. Let us now decompose the right–hand side of (8) as a summation of local error indicators η_κ over the elements κ in the computational mesh $\mathcal{T}_h$, i.e. we write

$$\begin{aligned} J(\mathbf{u}) - J(\mathbf{u}_h) = &- \mathcal{N}(\mathbf{u}_h, \mathbf{z} - \mathbf{z}_h) \equiv \sum_{\kappa \in \mathcal{T}_h} \eta_\kappa \\ &= \sum_{\kappa \in \mathcal{T}_h} \left\{ \int_\kappa \mathbf{R}(\mathbf{u}_h)(\mathbf{z} - \mathbf{z}_h)\, \mathrm{d}\mathbf{x} + \int_{\partial\kappa} \mathbf{r}(\mathbf{u}_h)(\mathbf{z} - \mathbf{z}_h)\, \mathrm{d}s \right\}, \end{aligned} \tag{9}$$

where $\mathbf{R}(\mathbf{u}_h)$ and $\mathbf{r}(\mathbf{u}_h)$ are element and face residuals of the discretization (2).

As in most cases the exact solution $\mathbf{z}$ to the dual problem (7) is not known, it is approximated numerically. However, (7) includes the unkown *exact* solution $\mathbf{u}$ to the primal problem. Thus, in order to approximate the dual solution $\mathbf{z}$, we must replace $\mathbf{u}$ in (7) by a suitable approximations. The linearizations leading to $\mathcal{M}(\mathbf{u}, \mathbf{u}_h; \cdot, \cdot)$ and $\bar{J}(\mathbf{u}, \mathbf{u}_h; \cdot)$ are performed about $\mathbf{u}_h$, resulting in $\mathcal{N}'_{\mathbf{u}}[\mathbf{u}_h](\cdot, \cdot)$ and $J'[\mathbf{u}_h](\cdot)$, respectively. The *linearized dual problem*: find $\hat{\mathbf{z}} \in \mathbf{V}$ such that

$$\mathcal{N}'_{\mathbf{u}}[\mathbf{u}_h](\mathbf{w}, \hat{\mathbf{z}}) = J'[\mathbf{u}_h](\mathbf{w}) \quad \forall \mathbf{w} \in \mathbf{V}, \tag{10}$$

is then discretized to yield following *approximate dual problem*: find $\hat{\mathbf{z}}_h \in \hat{\mathbf{V}}_h$ such that

$$\hat{\mathcal{N}}'_{\mathbf{u}}[\mathbf{u}_h](\mathbf{w}_h, \hat{\mathbf{z}}_h) = J'[\mathbf{u}_h](\mathbf{w}_h) \quad \forall \mathbf{w}_h \in \hat{\mathbf{V}}_h. \tag{11}$$

Replacing the dual solution $\mathbf{z}$ in (9) by its approximation $\hat{\mathbf{z}}_h$ results in following approximate error representation formula

$$J(\mathbf{u}) - J(\mathbf{u}_h) \approx -\mathcal{N}(\mathbf{u}_h, \hat{\mathbf{z}}_h - \mathbf{z}_h) \equiv \sum_{\kappa \in \mathcal{T}_h} \hat{\eta}_\kappa. \tag{12}$$

We note that the error introduced into the error representation through this replacement consists of the linearization and the discretization error of the dual problem, see [6] for a more detailed discussion. Furthermore, we note that the indicators $\hat{\eta}_\kappa$ are used for goal-oriented (adjoint-based) refinement. Finally, based on the error representation (9) given in terms of element and face residuals, $\mathbf{R}(\mathbf{u}_h)$ and $\mathbf{r}(\mathbf{u}_h)$, respectively, we can derive residual-based indicators, which do not require the solution of the adjoint problem (11).

In the following two Sections 3 and 4, we introduce the Discontinuous Galerkin (DG) discretization of the compressible Euler equations and the Interior Penalty DG discretization of the compressible Navier-Stokes equations and give the corresponding residual-based and adjoint-based refinement indicators which will be used in Section 5 for adaptive mesh refinement.

3 THE COMPRESSIBLE EULER EQUATIONS

We consider the two-dimensional steady state compressible Euler equations of gas dynamics given by

$$\nabla \cdot \mathcal{F}^c(\mathbf{u}) = 0 \quad \text{in } \Omega, \tag{13}$$

where $\Omega \in \mathbb{R}^2$ is an open bounded domain, $\mathcal{F}^c(\mathbf{u}) = (\mathbf{f}_1^c(\mathbf{u}), \mathbf{f}_2^c(\mathbf{u}))$, and the vector of conservative variables $\mathbf{u}$ and the convective fluxes $\mathbf{f}_i^c$, $i = 1, 2$, are defined by

$$\mathbf{u} = \begin{bmatrix} \rho \\ \rho v_1 \\ \rho v_2 \\ \rho E \end{bmatrix}, \quad \mathbf{f}_1^c(\mathbf{u}) = \begin{bmatrix} \rho v_1 \\ \rho v_1^2 + p \\ \rho v_1 v_2 \\ \rho H v_1 \end{bmatrix} \text{ and } \mathbf{f}_2^c(\mathbf{u}) = \begin{bmatrix} \rho v_2 \\ \rho v_1 v_2 \\ \rho v_2^2 + p \\ \rho H v_2 \end{bmatrix}, \tag{14}$$

where ρ, $\mathbf{v} = (v_1, v_2)^T$, p and E denote the density, velocity vector, pressure and specific total energy, respectively. Additionally, H is the total enthalpy given by

$$H = E + \frac{p}{\rho} = e + \tfrac{1}{2}\mathbf{v}^2 + \frac{p}{\rho}, \tag{15}$$

where e is the specific static internal energy, and the pressure is determined by the equation of state of an ideal gas, $p = (\gamma - 1)\rho e$, where $\gamma = c_p/c_v$ is the ratio of specific heat capacities at constant pressure, c_p, and constant volume, c_v; for dry air, $\gamma = 1.4$.

Given a subdivision of Ω into shape-regular meshes $\mathcal{T}_h = \{\kappa\}$ consisting of quadrilateral elements κ, and mappings σ_κ, $\kappa \in \mathcal{T}_h$ with $\kappa = \sigma_\kappa(\hat{\kappa})$ where $\hat{\kappa}$ is the reference (unit) square, we define the finite element space $\mathbf{V}_h^p$ of discontinuous piecewise vector-valued polynomial functions of degree $p \geq 0$ by

$$\mathbf{V}_h^p = \{\mathbf{v}_h \in [L_2(\Omega)]^m : \mathbf{v}_h|_\kappa \circ \sigma_\kappa \in [\mathcal{Q}_p(\hat{\kappa})]^m\}, \tag{16}$$

where $\mathcal{Q}_p(\hat{\kappa})$ denotes the space of tensor product polynomials of degree $p \geq 0$. Suppose that $\mathbf{v}|_\kappa \in [H^1(\kappa)]^m$ for each $\kappa \in \mathcal{T}_h$. Given an element $\kappa \in \mathcal{T}_h$ and neighoring element $\kappa' \in \mathcal{T}_h$ with $e = \partial\kappa \cap \kappa' \neq 0$, by $\mathbf{v}_\kappa^\pm$ (or $\mathbf{v}^\pm$ for short) we denote the traces of $\mathbf{v}$ taken from within the interior of κ and κ', respectively. The discontinuous Galerkin discretization of degree $p \geq 0$ of problem (13) is given by: Find $\mathbf{u}_h \in \mathbf{V}_h^p$ such that

$$\mathcal{N}(\mathbf{u}_h, \mathbf{v}_h) \equiv \sum_{\kappa \in \mathcal{T}_h} \left\{ -\int_\kappa \mathcal{F}^c(\mathbf{u}_h) : \nabla \mathbf{v}_h \, \mathrm{d}\mathbf{x} + \int_{\partial\kappa} \mathcal{H}(\mathbf{u}_h^+, \mathbf{u}_h^-, \mathbf{n}) \, \mathbf{v}_h^+ \, ds \right\} = 0 \tag{17}$$

for all $\mathbf{v}_h \in \mathbf{V}_h^p$, where $\mathcal{H}(\cdot, \cdot, \cdot)$ is a consistent and conservative numerical flux function, see [8] for more details. Substituting the semilinear form $\mathcal{N}(\mathbf{u}_h, \mathbf{v}_h)$ given in (17) into the error representation formula (9) and using integration by parts, we see that the adjoint-based indicators η_κ in (9) are defined by

$$\eta_\kappa = -\int_\kappa (\nabla \cdot \mathcal{F}^c(\mathbf{u}_h)) \cdot (\mathbf{z} - \mathbf{z}_h) \, \mathrm{d}\mathbf{x} + \int_{\partial\kappa} \left(\mathcal{F}^c(\mathbf{u}_h^+) \cdot \mathbf{n} - \mathcal{H}(\mathbf{u}_h^+, \mathbf{u}_h^-, \mathbf{n}) \right) \cdot (\mathbf{z} - \mathbf{z}_h) \, \mathrm{d}s, \tag{18}$$

and the element and face residuals in (9) are given by

$$\mathbf{R}(\mathbf{u}_h) = -\nabla \cdot \mathcal{F}^c(\mathbf{u}_h), \qquad \mathbf{r}(\mathbf{u}_h) = \mathcal{F}^c(\mathbf{u}_h^+) \cdot \mathbf{n} - \mathcal{H}(\mathbf{u}_h^+, \mathbf{u}_h^-, \mathbf{n}), \tag{19}$$

respectively. Finally, supposing that $\mathbf{z} \in [H^1(\Omega)]^4$, and there is a constant C_{stab} such that $\|\mathbf{z}\|_{H^1(\Omega)} \leq C_{\text{stab}}$, we can derive, see [8, 11], following residual-based indicators

$$\eta_\kappa^{\text{res}} = \|h\mathbf{R}(\mathbf{u}_h)\|_{L_2(\kappa)} + \|h^{1/2}\mathbf{r}(\mathbf{u}_h)\|_{L_2(\partial\kappa)}\,. \tag{20}$$

4 THE COMPRESSIBLE NAVIER-STOKES EQUATIONS

We consider the two–dimensional steady state compressible Navier-Stokes equations. Like in Section 3, ρ, $\mathbf{v} = (v_1, v_2)^T$, p and E denote the density, velocity vector, pressure and specific total energy, respectively. Furthermore, T denotes the temperature. The equations of motion are given by

$$\nabla \cdot (\mathcal{F}^c(\mathbf{u}) - \mathcal{F}^v(\mathbf{u}, \nabla\mathbf{u})) \equiv \frac{\partial}{\partial x_i}\mathbf{f}_i^c(\mathbf{u}) - \frac{\partial}{\partial x_i}\mathbf{f}_i^v(\mathbf{u}, \nabla\mathbf{u}) = 0 \quad \text{in } \Omega. \tag{21}$$

The vector of conservative variables $\mathbf{u}$ and the convective fluxes $\mathbf{f}_i^c$, $i = 1, 2$, are given by (14). Furthermore, the viscous fluxes $\mathbf{f}_i^v$, $i = 1, 2$, are defined by

$$\mathbf{f}_1^v(\mathbf{u}, \nabla\mathbf{u}) = \begin{bmatrix} 0 \\ \tau_{11} \\ \tau_{21} \\ \tau_{1j}v_j + \mathcal{K}T_{x_1} \end{bmatrix} \quad \text{and} \quad \mathbf{f}_2^v(\mathbf{u}, \nabla\mathbf{u}) = \begin{bmatrix} 0 \\ \tau_{12} \\ \tau_{22} \\ \tau_{2j}v_j + \mathcal{K}T_{x_2} \end{bmatrix}, \tag{22}$$

respectively, where $\mathcal{K}$ is the thermal conductivity coefficient. Finally, the viscous stress tensor is defined by

$$\tau = \mu\left(\nabla\mathbf{v} + (\nabla\mathbf{v})^T - \tfrac{2}{3}(\nabla \cdot \mathbf{v})I\right), \tag{23}$$

where μ is the dynamic viscosity coefficient, and the temperature T is given by $e = c_v T$; thus

$$\mathcal{K}T = \tfrac{\mu\gamma}{Pr}\left(E - \tfrac{1}{2}\mathbf{v}^2\right), \tag{24}$$

where $Pr = 0.72$ is the Prandtl number. Finally, we note that the viscous flux $\mathcal{F}^v(\mathbf{u}, \nabla\mathbf{u})$ is homogeneous with respect to the gradient of conservative variables $\nabla\mathbf{u}$, i.e. $\mathbf{f}_i^v(\mathbf{u}, \nabla\mathbf{u}) = G_{ij}(\mathbf{u})\partial\mathbf{u}/\partial x_j$, $i = 1, 2$, where G denotes the homogeneity tensor and is given by $G_{ij}(\mathbf{u}) = \partial\mathbf{f}_i^v(\mathbf{u}, \nabla\mathbf{u})/\partial u_{x_j}$, for $i, j = 1, 2$.

In addition to the notation introduced in Section 3, we now define average and jump operators. To this end, let κ^+ and κ^- be two adjacent elements of $\mathcal{T}_h$ and $\mathbf{x}$ be an arbitrary point on the interior edge $e = \partial\kappa^+ \cap \partial\kappa^- \subset \Gamma_{\mathcal{I}}$, where $\Gamma_{\mathcal{I}}$ denotes the union of all interior edges of $\mathcal{T}_h$. Moreover, let $\mathbf{v}$ and $\underline{\tau}$ be vector- and matrix-valued functions, respectively, that are smooth inside each element $\kappa^\pm$. By $(\mathbf{v}^\pm, \underline{\tau}^\pm)$ we denote the traces of $(\mathbf{v}, \underline{\tau})$ on e taken from within the interior of $\kappa^\pm$, respectively. Then, we define the averages

at $\mathbf{x} \in e$ by $\{\!\{\mathbf{v}\}\!\} = (\mathbf{v}^+ + \mathbf{v}^-)/2$ and $\{\!\{\underline{\tau}\}\!\} = (\underline{\tau}^+ + \underline{\tau}^-)/2$. Similarly, the jump at $\mathbf{x} \in e$ is given by $\underline{[\![\mathbf{v}]\!]} = \mathbf{v}^+ \otimes \mathbf{n}_{\kappa^+} + \mathbf{v}^- \otimes \mathbf{n}_{\kappa^-}$. On a boundary edge $e \subset \Gamma$, we set $\{\!\{\mathbf{v}\}\!\} = \mathbf{v}$, $\{\!\{\underline{\tau}\}\!\} = \underline{\tau}$ and $\underline{[\![\mathbf{v}]\!]} = \mathbf{v} \otimes \mathbf{n}$. For matrices $\underline{\sigma}, \underline{\tau} \in \mathbb{R}^{m \times n}$, $m, n \geq 1$, we use the standard notation $\underline{\sigma} : \underline{\tau} = \sum_{k=1}^{m} \sum_{l=1}^{n} \sigma_{kl} \tau_{kl}$; additionally, for vectors $\mathbf{v} \in \mathbb{R}^m, \mathbf{w} \in \mathbb{R}^n$, the matrix $\mathbf{v} \otimes \mathbf{w} \in \mathbb{R}^{m \times n}$ is defined by $(\mathbf{v} \otimes \mathbf{w})_{kl} = v_k \, w_l$.

The interior penalty discontinuous Galerkin discretization of the compressible Navier-Stokes equations is given, [9], by

$$
\begin{aligned}
\mathcal{N}(\mathbf{u}_h, \mathbf{v}_h) \equiv & - \int_\Omega \mathcal{F}^c(\mathbf{u}_h) : \nabla_h \mathbf{v}_h \, \mathrm{d}\mathbf{x} + \sum_{\kappa \in \mathcal{T}_h} \int_{\partial\kappa \setminus \Gamma} \mathcal{H}(\mathbf{u}_h^+, \mathbf{u}_h^-, \mathbf{n}_\kappa) \cdot \mathbf{v}_h^+ \, \mathrm{d}s \\
& + \int_\Omega \mathcal{F}^v(\mathbf{u}_h, \nabla_h \mathbf{u}_h) : \nabla_h \mathbf{v}_h \, \mathrm{d}\mathbf{x} - \int_{\Gamma_\mathcal{I}} \{\!\{ \mathcal{F}^v(\mathbf{u}_h, \nabla_h \mathbf{u}_h) \}\!\} : \underline{[\![\mathbf{v}_h]\!]} \, \mathrm{d}s \\
& - \int_{\Gamma_\mathcal{I}} \{\!\{ \left(G_{i1}^T \partial_h \mathbf{v}_h / \partial x_i, G_{i2}^T \partial_h \mathbf{v}_h / \partial x_i \right) \}\!\} : \underline{[\![\mathbf{u}_h]\!]} \, \mathrm{d}s \\
& + \int_{\Gamma_\mathcal{I}} \delta \underline{[\![\mathbf{u}_h]\!]} : \underline{[\![\mathbf{v}_h]\!]} \, \mathrm{d}s + \mathcal{N}_\Gamma(\mathbf{u}_h, \mathbf{v}_h),
\end{aligned}
\tag{25}
$$

where $\mathcal{N}_\Gamma(\mathbf{u}_h, \mathbf{v}_h)$ includes all boundary terms, see [9] for more details.

Substituting the semilinear form $\mathcal{N}(\mathbf{u}_h, \mathbf{v}_h)$ given in (25) into the error representation formula (9) and, again, using integration by parts, we see that the adjoint-based indicators η_κ in (9) are given by

$$
\begin{aligned}
\eta_\kappa = & \int_\kappa (-\nabla \cdot \mathcal{F}^c(\mathbf{u}_h) + \nabla \cdot \mathcal{F}^v(\mathbf{u}_h, \nabla \mathbf{u}_h)) \cdot (\mathbf{z} - \mathbf{z}_h) \, \mathrm{d}\mathbf{x} \\
& + \int_{\partial\kappa \setminus \Gamma} (\mathcal{F}^c(\mathbf{u}_h) \cdot \mathbf{n}_\kappa - \mathcal{H}(\mathbf{u}_h^+, \mathbf{u}_h^-, \mathbf{n}_\kappa)) \cdot (\mathbf{z} - \mathbf{z}_h)^+ \, \mathrm{d}s \\
& + \frac{1}{2} \int_{\partial\kappa \setminus \Gamma} \left(G_{i1}^\top \partial_h (\mathbf{z} - \mathbf{z}_h) / \partial x_i, G_{i2}^\top \partial_h (\mathbf{z} - \mathbf{z}_h) / \partial x_i \right) : \underline{[\![\mathbf{u}_h]\!]} \, \mathrm{d}s \\
& - \frac{1}{2} \int_{\partial\kappa \setminus \Gamma} [\![\mathcal{F}^v(\mathbf{u}_h, \nabla \mathbf{u}_h)]\!] \cdot (\mathbf{z} - \mathbf{z}_h)^+ \, \mathrm{d}s - \int_{\partial\kappa \setminus \Gamma} \delta \underline{[\![\mathbf{u}_h]\!]} : (\mathbf{z} - \mathbf{z}_h)^+ \otimes \mathbf{n}_\kappa \, \mathrm{d}s + \eta_{\partial\kappa \cap \Gamma},
\end{aligned}
$$

where $\eta_{\partial\kappa\cap\Gamma}$ includes the residual contributions of the boundary terms $\mathcal{N}_\Gamma(\mathbf{u}_h, \mathbf{v}_h)$, see [10] for more detail. Finally, supposing that $\mathbf{z} \in [H^s(\Omega)]^4$, $2 \leq s \leq p+1$, and that there is a constant C_{stab} such that $\|\mathbf{z}\|_{H^s(\Omega)} \leq C_{\mathrm{stab}}$, we can derive, cf. [10], following residual-based indicators

$$
\begin{aligned}
\eta_\kappa^{\mathrm{res}} = & \|h_\kappa^s \mathbf{R}(\mathbf{u}_h)\|_{L_2(\kappa)} + \|h_\kappa^{s-1/2} (\mathcal{F}^c(\mathbf{u}_h) \cdot \mathbf{n}_\kappa - \mathcal{H}(\mathbf{u}_h^+, \mathbf{u}_h^-, \mathbf{n}_\kappa))\|_{L_2(\partial\kappa \setminus \Gamma)} \\
& + \|h_\kappa^{s-3/2} G_{\cdot j} \underline{[\![\mathbf{u}_h]\!]}_j \|_{L_2(\partial\kappa \setminus \Gamma)} + \|h_\kappa^{s-1/2} [\![\mathcal{F}^v(\mathbf{u}_h, \nabla \mathbf{u}_h)]\!] \|_{L_2(\partial\kappa \setminus \Gamma)} \\
& + \|h_\kappa^{s-1/2} \delta \left(\mathbf{u}_h^+ - \mathbf{u}_h^- \right) \|_{L_2(\partial\kappa \setminus \Gamma)} + \eta_{\partial\kappa\cap\Gamma}^{\mathrm{res}},
\end{aligned}
\tag{26}
$$

where $\mathbf{R}(\mathbf{u}_h) = -\nabla \cdot \mathcal{F}^c(\mathbf{u}_h) + \nabla \cdot \mathcal{F}^v(\mathbf{u}_h, \nabla \mathbf{u}_h)$ denotes the element residual, and $\eta_{\partial\kappa\cap\Gamma}^{\mathrm{res}}$ includes the contributions of boundary residual terms to the indicator.

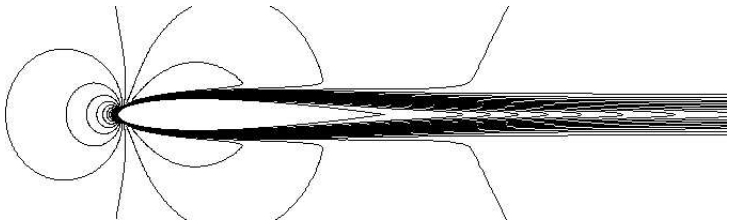

Figure 1: Mach isolines of the $M = 0.5, \mathrm{Re} = 5000, \alpha = 0^\circ$ flow around the NACA0012 airfoil.

5 NUMERICAL EXAMPLES

In this Section we give two numerical examples demonstrating that the approximate error representation $-\mathcal{N}(\mathbf{u}_h, \hat{\mathbf{z}}_h - \mathbf{z}_h) = \sum_{\kappa \in \mathcal{T}_h} \hat{\eta}_\kappa$, cf. (12), which was derived from the (exact) error representation (9) by replacing the dual solution $\mathbf{z}$ by an approximate dual solution $\hat{\mathbf{z}}_h$, gives a good approximation to the true error measured in terms of the specific target quantity $J(\mathbf{u})$. Furthermore, we show that using the approximate error representation, an improved value of the target functional, namely, $\tilde{J}(\mathbf{u}_h) = J(\mathbf{u}_h) + \sum_{\kappa \in \mathcal{T}_h} \hat{\eta}_\kappa$ can be obtained. Finally, we highlight the advantages of designing an adaptive finite element algorithm based on the *adjoint-based* indicators $\hat{\eta}_\kappa$, in comparison to *residual-based* indicators $\eta_\kappa^{\mathrm{res}}$, which do not require the solution of an adjoint problem.

First, we consider the example, see [10], of a subsonic viscous flow ($M = 0.5, \mathrm{Re} = 5000, \alpha = 0^\circ$) around the NACA0012 airfoil with an adiabatic no-slip boundary condition imposed on the profile, see Figure 1. In Table 1 we demonstrate the performance of the adaptive algorithm for the numerical approximation of the viscous drag coefficient $J(\mathbf{u}) = J_{c_{\mathrm{df}}}(\mathbf{u}) = \frac{2}{l\bar{\rho}|\bar{\mathbf{v}}|^2} \int_S (\underline{\tau}\,\mathbf{n}) \cdot \psi_d \, \mathrm{d}s$ with $\psi_d = (1,0)^\top$, when employing the adjoint-based indicators $\hat{\eta}_\kappa$. Here, we show the number of elements and degrees of freedom (DoF) in $\mathbf{V}_h$, the true error in the functional $J(\mathbf{u}) - J(\mathbf{u}_h)$ based on a reference value $J_{c_{\mathrm{df}}}(\mathbf{u}) \approx 0.032535$, the computed error representation formula and its effectivity index $\theta = \sum_{\kappa \in \mathcal{T}_h} \hat{\eta}_\kappa / (J(\mathbf{u}) - J(\mathbf{u}_h))$. We see that initially on very coarse meshes the quality of the computed error representation formula $\sum_{\kappa \in \mathcal{T}_h} \hat{\eta}_\kappa$ is rather poor, in the sense that θ noticeably differs from one; however, as the mesh is refined, we observe that the effectivity indices θ slowly tend towards unity.

In Figure 2 we compare the true error in the computed target functional $J_{c_{\mathrm{df}}}(\cdot)$ using a mesh refinement strategy based on the residual-based indicators $\eta_\kappa^{\mathrm{res}}$ and a mesh refinement strategy based on the adjoint-based indicators $\hat{\eta}_\kappa$. Here, we clearly observe the superiority of employing the adjoint-based indicator; on the final mesh, the true error in the computed target functional is almost 2 orders of magnitude smaller than $|J_{c_{\mathrm{df}}}(\mathbf{u}) - J_{c_{\mathrm{df}}}(\mathbf{u}_h)|$ computed on the sequence of meshes produced using $\eta_\kappa^{\mathrm{res}}$. Moreover, here we also show the error in the improved value of the viscous drag coefficient, i.e. $|J_{c_{\mathrm{df}}}(\mathbf{u}) - \tilde{J}_{c_{\mathrm{df}}}(\mathbf{u}_h)|$; in this case, we clearly see that this error is of higher–order than the baseline error $|J_{c_{\mathrm{df}}}(\mathbf{u}) - J_{c_{\mathrm{df}}}(\mathbf{u}_h)|$. Indeed, on the finest mesh the error in the improved target functional is over an order

Table 1: $M = 0.5, \mathrm{Re} = 5000, \alpha = 0^\circ$ flow around the NACA0012 airfoil: Adaptive algorithm for the numerical approximation of c_{df} based on employing adjoint-based indicator $\hat{\eta}_\kappa$.

Elements	DoF	$J(\mathbf{u}) - J(\mathbf{u}_h)$	$\sum_{\kappa \in \mathcal{T}_h} \hat{\eta}_\kappa$	θ
3072	49152	-1.839e-02	-1.274e-02	0.69
4962	79392	-3.680e-03	-3.239e-03	0.88
8028	128448	-8.246e-04	-7.596e-04	0.92
13446	215136	-1.773e-04	-1.680e-04	0.95
21750	348000	-4.444e-05	-4.258e-05	0.96
35118	561888	-1.624e-05	-1.626e-05	1.00

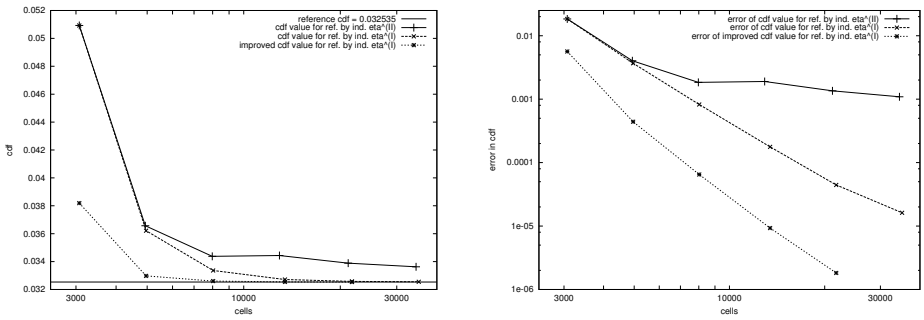

(a) (b)

Figure 2: $M = 0.5, \mathrm{Re} = 5000, \alpha = 0^\circ$ flow around the NACA0012 airfoil: (a) Computed values of c_{df} based on employing the adjoint-based indicator ($\texttt{eta}^{(\mathrm{I})}$) and the residual-based indicator ($\texttt{eta}^{(\mathrm{II})}$), together with the improved value; (b) Convergence of the error in these quantities.

of magnitude smaller than the corresponding quantity computed with the adjoint-based indicator. We also point out that after just one mesh refinement step, the improved value $\tilde{J}_{c_{\mathrm{df}}}(\mathbf{u}_h)$ computed on the mesh refined using the adjoint-based indicator is more accurate than the corresponding value $J_{c_{\mathrm{df}}}(\mathbf{u}_h)$ computed on the *finest* mesh designed on the basis of employing the residual-based indicator.

In a second example, cf. [6], we consider a supersonic horizontal viscous flow at $M = 1.2$ and $\mathrm{Re} = 1000$ around the NACA0012 airfoil, with an adiabatic no-slip boundary condition imposed on the profile, see Figure 3. In order to avoid overshoots near the bow shock, we add a consistent shock-capturing term, see [6], to the discretization (25). In this example, we now consider the approximation of the pressure induced drag, c_{dp}, i.e. the target quantity is $J(\mathbf{u}) = J_{c_{\mathrm{dp}}}(\mathbf{u}) = \frac{2}{l\bar{\rho}|\bar{\mathbf{v}}|^2} \int_S p\,(\mathbf{n} \cdot \psi_d)\,\mathrm{d}s$, with $\psi_d = (1,0)^\top$.

In Table 2 we collect the data of the adaptive refinement algorithm when the adjoint-based indicators are employed. Again, we see that from the second mesh onwards, the approximate error representation $\sum_\kappa \hat{\eta}_\kappa$ is very close to the true error $J(\mathbf{u}) - J(\mathbf{u}_h)$ based on the reference value $J_{c_{\mathrm{dp}}}(\mathbf{u}) \approx 0.10109$.

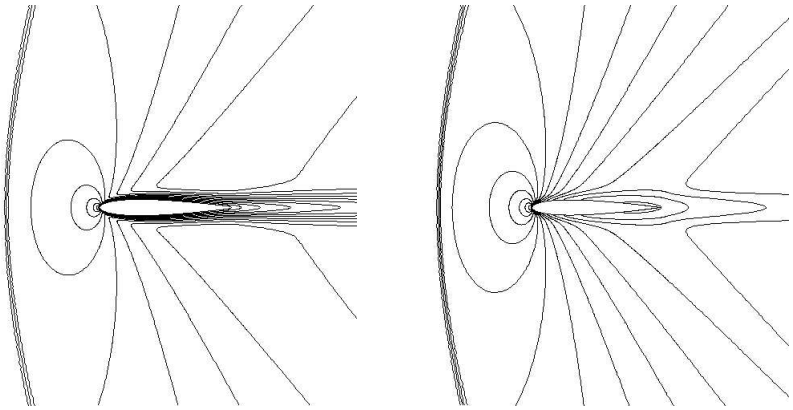

(a) (b)

Figure 3: $M = 1.2, \mathrm{Re} = 1000, \alpha = 0^\circ$ flow around the NACA0012 airfoil: (a) Mach isolines and (b) density isolines.

# el.	# DoFs	$J(\mathbf{u}) - J(\mathbf{u}_h)$	$\sum_\kappa \hat{\eta}_\kappa$	θ
768	12288	-1.363e-02	-6.312e-03	0.46
1260	20160	-3.203e-03	-2.995e-03	0.94
2154	34464	-4.844e-04	-5.368e-04	1.11
3570	57120	-3.474e-04	-3.333e-04	0.96
6021	96336	-1.835e-04	-1.856e-04	1.01
10038	160608	-1.644e-04	-1.653e-04	1.01

Table 2: Viscous $M = 1.2, \mathrm{Re} = 1000, \alpha = 0^\circ$ flow around the NACA0012 airfoil: Adaptive algorithm for the accurate approximation of c_{dp}.

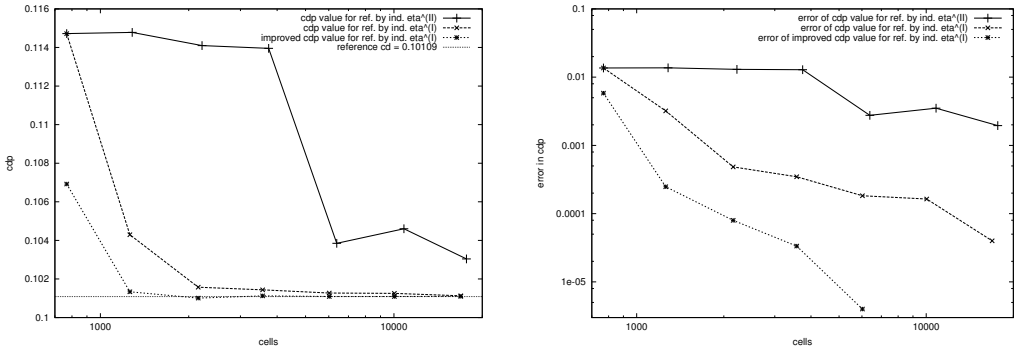

(a) (b)

Figure 4: $M = 1.2, \mathrm{Re} = 1000, \alpha = 0^\circ$ flow around the NACA0012 airfoil: (a) Computed values of c_{df} based on employing the adjoint-based indicator ($\texttt{eta}^{(\mathrm{I})}$) and the residual-based indicator ($\texttt{eta}^{(\mathrm{II})}$), together with the improved value; (b) Convergence of the error in these quantities.

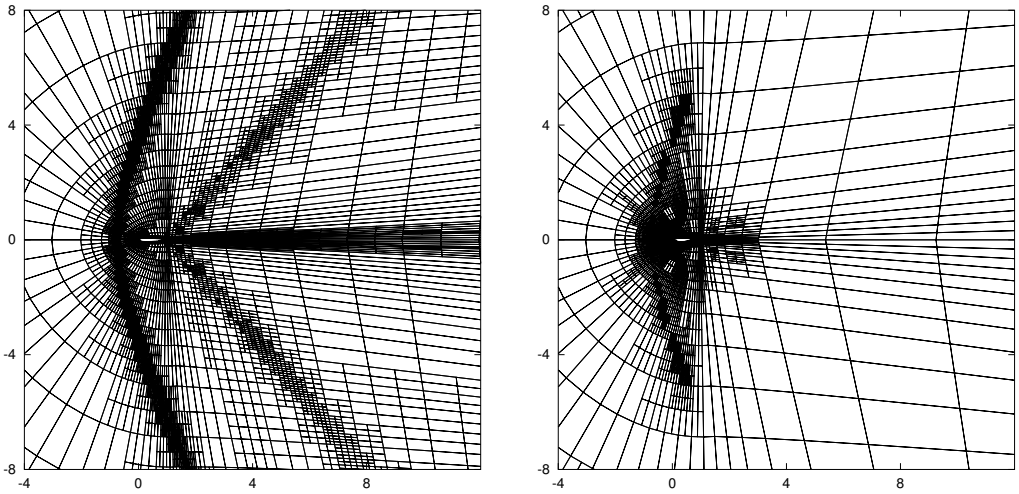

Figure 5: $M = 1.2, \mathrm{Re} = 1000, \alpha = 0^\circ$ flow around the NACA0012 airfoil: (a) residual-based refined mesh of 17670 elements with 282720 degrees of freedom and $|J_{c_{\mathrm{dp}}}(\mathbf{u}) - J_{c_{\mathrm{dp}}}(\mathbf{u}_h)| = 1.9 \cdot 10^{-3}$; (b) adjoint-based refined mesh for c_{dp}: mesh of 10038 elements with 160608 degrees of freedom and $|J_{c_{\mathrm{dp}}}(\mathbf{u}) - J_{c_{\mathrm{dp}}}(\mathbf{u}_h)| = 1.6 \cdot 10^{-4}$.

In Figure 4 we compare the true error in the target quantity for the two mesh refinement strategies based on the adjoint-based indicator $\hat{\eta}_\kappa$ and on the residual-based indicator $\eta_\kappa^{\mathrm{res}}$, respectively. We see, that on the first three refinement steps when employing the residual-based indicator the accuracy in the target quantity is hardly improved. In contrast to that, when using adjoint-based indicators, the error decreases significantly faster, being a factor of more than three smaller already after the second refinement step than the error on the finest residual-based refined mesh. Furthermore, in Figure 4 we see, that the improved values, $\tilde{J}(\mathbf{u}_h)$, are significantly more accurate than the (baseline) $J(\mathbf{u}_h)$ values, and even show a higher rate of convergence, see [6] for a more detailed discussion.

The large difference in the performance, see Figure 4, of the adjoint-based indicators and the residual-based indicators in producing adaptively refined meshes for the accurate approximation of the target quantity c_{dp}, is due to the very different parts of the computational meshes being marked for refinement by the two types of indicators. Figure 5 (a) shows the finest mesh produced by employing the residual-based indicator. We see, that this refinement criterion aims at resolving all flow features: the extensive bow shock, the wake of the flow behind the airfoil as well as the weak shocks emanating from the trailing edge of the airfoil. In contrast to that, the refinement of the mesh produced by employing the adjoint-based indicator, see Figures 5 (b), is very concentrated close to the airfoil. In particular, the bow shock is mainly resolved in a small region upstream of the profile only, and there is no refinement at the position of the bow shock beyond six chord lengths above and below the profile. Furthermore, the weak shocks emanating from the

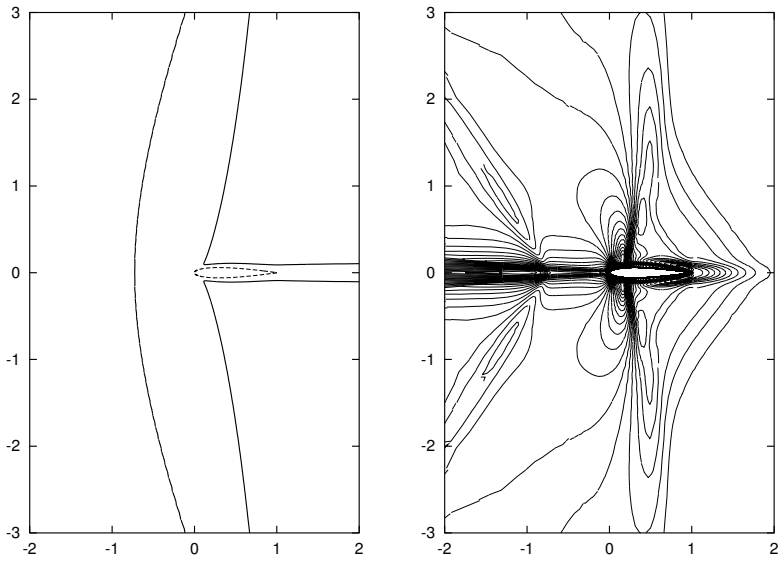

Figure 6: Viscous flow at $M = 1.2, \mathrm{Re} = 1000, \alpha = 0^\circ$ around the NACA0012 airfoil: (a) Sonic isolines of the flow solution; (b) isolines of the $\hat{z}_1$ component of the computed adjoint solution $\hat{\mathbf{z}}$.

trailing edge are not resolved and there is no refinement in the wake of the flow beyond three chord lengths behind the profile. Instead, the refinement of the mesh is concentrated near the leading edge of the profile and in the boundary layer of the flow. All other parts of the computational domain are recognized by the adjoint-based indicator to be of minor importance for the accuracy of the c_{dp} target quantity. In fact, the dual (adjoint) solution, see Figure 6, includes the crucial information concerning which local residuals contribute to the error in the target quantity and to what extent. Herewith, it offers all necessary information of error transport and accumulation. Finally, the adjoint-based indicators mark only those parts of the domain for refinement where residuals of the flow solution significantly contribute to the error of the target quantity, i.e. all parts which are important for the accurate approximation of the target quantity.

6 CONCLUSION AND OUTLOOK

In this article, we have given an overview of recent developments in error estimation as well as in residual-based and goal-oriented (adjoint-based) adaptation for Discontinuous Galerkin discretizations of sub- and supersonic viscous compressible flows. In particular, after presenting an overview of the general theoretical framework of duality-based (adjoint-based) *a posteriori* error estimation, we have introduced the Discontinuous Galerkin (DG) discretization of the compressible Euler equations and the Interior Penalty DG discretization of the compressible Navier-Stokes equations and have given the corre-

sponding residual-based and adjoint-based refinement indicators used for adaptive mesh refinement. We have demonstrated for a subsonic and a supersonic viscous compressible flow that a reliable error estimation is obtained with respect to specific target quantities like aerodynamical force coefficients. Furthermore, we have shown that the error estimation can be used to obtain improved values (of higher order convergence) for the target quantities. Finally, we demonstrated that mesh refinement using adjoint-based indicators produces meshes which are specifically tailored to the efficient computation of the quantities of interest. It has been shown for a sub- and a supersonic viscous compressible flow that the adjoint-based mesh refinement leads to a several orders of magnitude improved accuracy compared to residual-based mesh refinement for the same number of points.

The results show that there is an enormous potential in the presented methods for improving the efficiency and reliability of aerodynamical simulations. However, significant effort will be required to make these methods usable in large-scale aerodynamical applications. To this end, in the context of the EU project ADIGMA ("Adaptive Higher-Order Variational Methods for Aerodynamic Applications in Industry") it is planned to extend these methods to turbulent compressible high Reynolds flows on complex 3d geometries, as is required for exploitation in industrial applications.

7 ACKNOWLEGMENTS

This work has been supported by the President's Initiative and Networking Fund of the Helmholtz Association of German Research Centres.

REFERENCES

[1] R. Becker and R. Rannacher. A feed-back approach to error control in finite element methods: Basic analysis and examples. *East–West J. Numer. Math.*, 4:237–264, 1996.

[2] R. Becker and R. Rannacher. An optimal control approach to error estimation and mesh adaptation in finite element methods. *Acta Numerica*, 10:1–102, 2001.

[3] K. Eriksson, D. Estep, P. Hansbo, and C. Johnson. Introduction to adaptive methods for differential equations. *Acta Numerica*, pages 105–158, 1995.

[4] R. Hartmann. Adaptive FE Methods for Conservation Equations. In H. Freistühler and G. Warnecke, editors, *Hyperbolic Problems: theory, numerics, applications: eighth international conference in Magdeburg, February, March 2000*, volume 141 of *International series of numerical mathematics*, pages 495–503. Birkhäuser, Basel, 2001.

[5] R. Hartmann. *Adaptive Finite Element Methods for the Compressible Euler Equations*. PhD thesis, University of Heidelberg, 2002.

[6] R. Hartmann. Adaptive discontinuous Galerkin methods with shock-capturing for the compressible Navier-Stokes equations. *Int. J. Numer. Meth. Fluids*, 2006. To appear.

[7] R. Hartmann and P. Houston. Adaptive discontinuous Galerkin finite element methods for nonlinear hyperbolic conservation laws. *SIAM J. Sci. Comp.*, 24:979–1004, 2002.

[8] R. Hartmann and P. Houston. Adaptive discontinuous Galerkin finite element methods for the compressible Euler equations. *J. Comp. Phys.*, 183:508–532, 2002.

[9] R. Hartmann and P. Houston. Symmetric interior penalty DG methods for the compressible Navier–Stokes equations I: Method formulation. *Int. J. Num. Anal. Model.*, 3(1):1–20, 2006.

[10] R. Hartmann and P. Houston. Symmetric interior penalty DG methods for the compressible Navier–Stokes equations II: Goal–oriented a posteriori error estimation. *Int. J. Num. Anal. Model.*, 3(2):141–162, 2006.

[11] P. Houston and E. Süli. *hp*–adaptive discontinuous Galerkin finite element methods for first–order hyperbolic problems. *SIAM J. Sci. Comp.*, 23(4):1225–1251, 2001.